Plant Stress 15 (2025) 100791

Contents lists available at ScienceDirect

Plant Stress

journal homepage: www.sciencedirect.com/journal/plant-stress

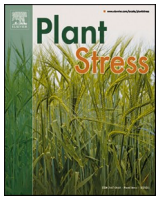

# Chloroplast positioning affects Hexokinase 1-mediated plant immunity under combined low temperature and high light

Sophia Bianca Bagshaw [a], Anastasia Kitashova [a], Beyza Özmen [a], Chun Kwan Yip [a], Bianca Emily Süling [a,b], Laura Schröder [a], Tatjana Kleine [c], Thomas Nägele [a,*]

[a] LMU München, Faculty of Biology, Plant Evolutionary Cell Biology, Großhaderner Str. 2-4, 82152 Planegg, Germany
[b] LMU München, Faculty of Biology, Plant Development, Großhaderner Str. 2-4, 82152 Planegg, Germany
[c] LMU München, Faculty of Biology, Plant Molecular Biology, Großhaderner Str. 2-4, 82152 Planegg, Germany

ARTICLE INFO

*Keywords:*
*Arabidopsis thaliana*
Cold acclimation
Chloroplast positioning
Carbohydrate metabolism
Plant immune response

ABSTRACT

Molecular networks involved in the responses of plants towards environmental changes are multifaceted and affect diverse metabolic and signalling pathways. Under challenging environmental conditions, such as low temperatures and high light intensities, plants need to immediately adjust their metabolism to prevent irreversible tissue damage. Regulation of photosynthesis and carbohydrate metabolism plays a crucial role in this stress response. Here, we analysed mutants of *Arabidopsis thaliana*, which were affected in either central enzymatic activities of carbohydrate metabolism, in chloroplast positioning or in a combination of both. Plants were exposed to a treatment of combined cold and elevated light. While mutants with deficiencies in sucrose or starch metabolism showed affected metabolic pathway regulation under abiotic stress, Hexokinase 1 mutants (*hxk1*) showed a severe growth phenotype with lesions and pale areas on leaf tissue. In a double mutant, combining deficiencies in Chloroplast Unusual Positioning 1 (CHUP1)-mediated chloroplast positioning and HXK1 (*hxk1 x chup1*), this growth phenotype vanished resulting in wild type-like plants. Transcriptome analysis revealed a significantly affected immune response of *hxk1* plants, which was suppressed in the double mutants. Our results support previous findings which suggested that HXK1 acts as a positive regulator of the plant immune response. Finally, we suggest that, due to its potential role as a negative regulator of plant immunity, CHUP1 deficiency counteracted the reduced immunity of *hxk1* in the double mutant which rescued the plants. Future studies might now reveal whether deficiencies in CHUP1 function and/or transcription represent a conserved strategy to increase plant immunity under abiotic stress.

## 1. Introduction

Plant carbohydrates are direct products of photosynthetic $CO_2$ assimilation. Within the Calvin-Benson-Bassham cycle (CBBc), ribulose-1,5-bisphosphate carboxylase/ oxygenase (Rubisco) enzymes catalyse both carboxylation and oxygenation reactions resulting in two or one molecule(s) of 3-phosphoglycerate, respectively. In the following reactions, which are ATP- and NADPH-dependent, triose phosphates are synthesised, which are substrates for either metabolic pathways or regeneration of CBBc intermediates. Both ATP and NADPH are synthesised within the primary photosynthetic reactions across thylakoid membranes in chloroplasts (Govindjee et al., 2017). To prevent an overaccumulation of ATP/NADPH and a depletion of ADP and $NADP^+$, a tight regulation of the photosynthetic electron transport and ATP/NADPH consumption in the CBBc is necessary. One way the activity of enzymes central to the CBBc can be regulated in response to the photosynthetic electron transport rate is via thioredoxins which, in a ferredoxin-dependent manner, affect the reduction state and the activity of their targets (Geigenberger et al., 2017). The carbohydrate metabolism in the chloroplast is also tightly connected with cytosolic pathways through mechanisms such as metabolite transport across the chloroplast envelope (Flügge, 1999; Patzke et al., 2019). An example of this is the translocation of plastidial triose phosphates in an antiport manner into the cytosol while inorganic phosphate is transported into the chloroplast which prevents phosphate depletion and deregulation of photosynthetic $CO_2$ assimilation (Flügge and Heldt, 1981). In the cytosol, sugar phosphates are substrates for energy metabolism, numerous metabolic pathways, sucrose biosynthesis, and biomass

* Corresponding author.
*E-mail address:* thomas.naegele@lmu.de (T. Nägele).

https://doi.org/10.1016/j.stress.2025.100791
Received 18 December 2024; Received in revised form 18 February 2025; Accepted 2 March 2025
Available online 3 March 2025

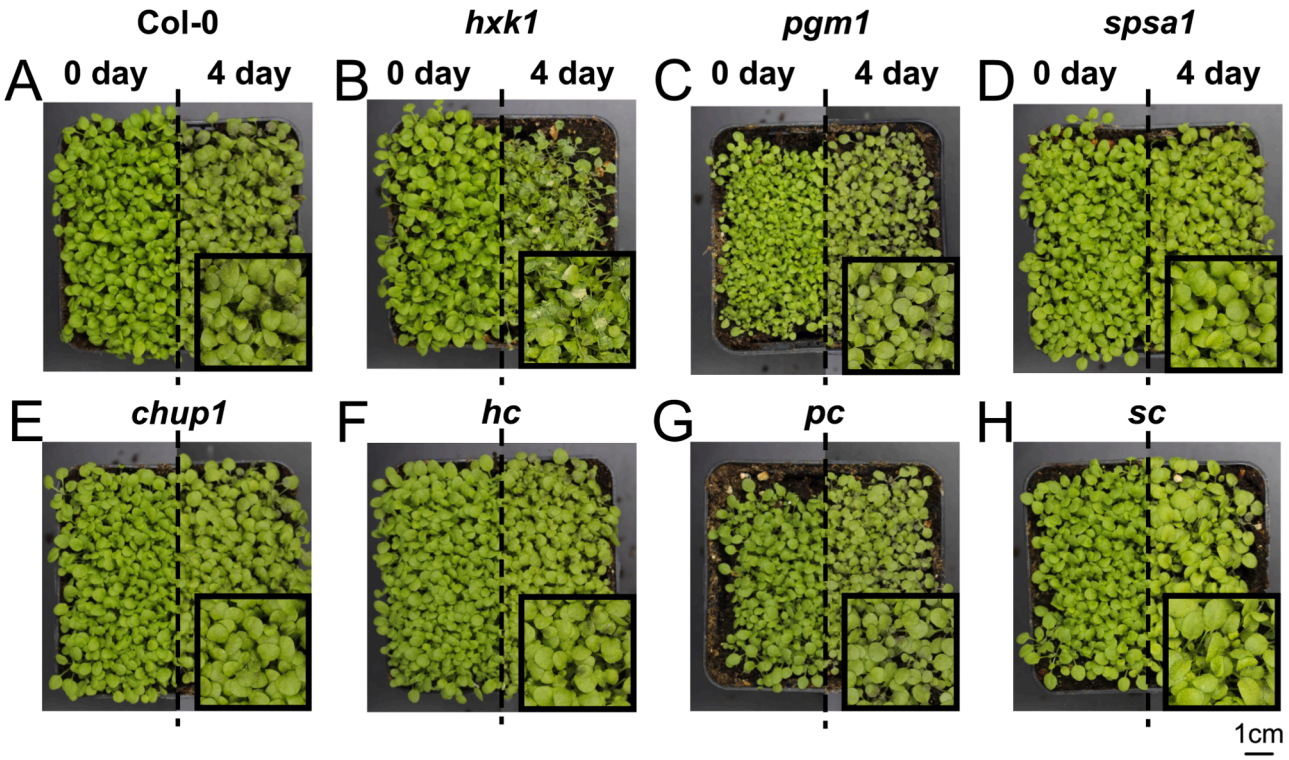


**Fig. 1.** Effects of deficiencies in CHUP1 and/or enzymatic activities on the growth phenotype. Each genotype is shown before (0 day) and after (4 day) exposure to combined cold/elevated light treatment (left/right). (A) Col-0, (B) *hxk1*, (C) *pgm1*, (D) *spsa1*, (E) *chup1*, (F) *hc (hxk1 x chup1)*, (G) *pc (pgm1 x chup1)*, (H) *sc (spsa1 x chup1)*. Magnifications in (B) shows the *hxk1* phenotype under LT/EL.

accumulation. Together with starch, sucrose represents the central product of photosynthesis and is, in many plant species, the most abundant transport sugar which supplies non-photosynthetic and below-ground leaf tissue with carbon equivalents (Braun, 2022).

Due to its central role in whole plant metabolism, stress tolerance and developmental processes, understanding the regulation of sucrose metabolism in a changing environment is important for many research areas. However, the experimental analysis of sucrose metabolism is aggravated by the diversity of factors that influence actual sucrose concentrations. The cyclic biosynthesis and breakdown of sucrose, catalysed by sucrose phosphate synthase, invertases, and hexokinases, challenges the interpretation of concentration dynamics (Nägele, 2022). Such dynamics are typically observed if environmental factors, like temperature or light intensity, change. Under low temperatures, sucrose concentrations significantly increase together with many other carbohydrates, amino acids and polyamines (Hannah et al., 2006; Guy et al., 2008; Hoermiller et al., 2022). These rising concentrations have been discussed in context of cryoprotection of membranes, where polar head groups, e.g., of carbohydrates and membrane lipids, are suggested to interact and prevent membrane fusion (Hincha et al., 2003). Further, chloroplast-located raffinose family oligosaccharides (RFOs) were shown to stabilize Photosystem II during freeze/thaw cycles, most probably due to stabilization of thylakoid membranes and/or membrane-localized proteins (Knaupp et al., 2011). Sucrose, together with galactinol, is substrate for RFO biosynthesis which again emphasises its multifaceted metabolic role in plant metabolism.

By relocating chloroplasts within a cell, plants can regulate electromagnetic energy absorption. Under high light intensities, in an avoidance response, chloroplasts are positioned along the anticlinal cell wall to reduce the total surface area of light absorption (Kasahara et al., 2002). In contrast, under low light intensities, chloroplasts accumulate perpendicular to the incident light to maximise absorption (accumulation response). The accumulation response was found to be mediated by blue light receptors Phototropin 1 and 2 (PHOT1 and 2; (Sakai et al., 2001)), while the avoidance response is mediated by PHOT2, which was also observed to affect chloroplast localization under low temperatures (Kagawa et al., 2001; Kodama et al., 2008). The organelle movement itself is catalysed by Chloroplast Unusual Positioning 1 (CHUP1) proteins, which represent plant-specific actin polymerization factors (Kong et al., 2024). Recent work suggested that chloroplast actin filaments, which are built at the interface between plasma membrane and chloroplasts, generate the motive force during chloroplast movement but detailed mechanisms remain to be elucidated (Wada and Kong, 2018; Kong et al., 2024). In addition to their function in photosynthesis, chloroplasts are also involved in sensing environmental stress (Richter et al., 2023). For example, chloroplasts integrate biotic and abiotic stress signalling through jasmonic acid biosynthesis, with jasmonic acid playing key roles in both biotic and abiotic stresses (Wang et al., 2021).

Due to the observations that (i) chloroplast positioning significantly affects photosynthetic performance, (ii) photosynthetic performance affects carbohydrate metabolism, and (iii) carbohydrate metabolism plays an essential role for acclimation to a changing environment, we analysed mutants of *Arabidopsis thaliana* which were either affected in enzyme activities of the central carbohydrate metabolism, in chloroplast positioning, or in a combination of both. Applying a combined elevated light and low temperature treatment revealed that Hexokinase 1 (HXK1) plays a central role for growth under such growth conditions which was linked to chloroplast positioning and plant immune response.

## 2. Materials and methods

### 2.1. Plant material and growth conditions

Plants of wild type *Arabidopsis thaliana*, accession Col-0, and seven mutants deficient in the chloroplast movement protein CHLOROPLAST UNUSUAL POSITIONING 1 (*chup1*, AT3G25690, SALK_129128C), plastidial phosphoglucomutase 1 (*pgm1*, AT5G51820, CS3092), cytosolic sucrose phosphate synthase A1 (*spsa1*, AT5G20280, SALK_148643C),

cytosolic hexokinase 1 (*hxk1*, AT4G29130, SALK_034233C), as well as double mutants *pgm1 x chup1 (pc), spsa1 x chup1 (sc)*, and *hxk1 x chup1 (hc)*, were grown on a 1:1 mixture of GS90 soil and vermiculite in a climate chamber under controlled short day conditions (8 h/16 h light/dark; 100 µmol $m^{-2}$ $s^{-1}$; 22 °C/16 °C; 60 % relative humidity). After two weeks, plants were transferred to a greenhouse and grown under long day conditions (16 h/8 h light/dark; 100 µmol $m^{-2}$ $s^{-1}$; 22 °C/16 °C; 60 % relative humidity). After one further week, seedlings were either (i) sampled at midday, i.e., after 8 h of light (0 days of acclimation), or (ii) transferred to a cold room for low temperature and elevated light treatment (LT/EL; 16 h/8 h light/ dark; 250 µmol $m^{-2}$ $s^{-1}$; 4 °C/4 °C). LT/EL exposed plants were sampled after 4 days at midday, i.e., after 8 h of light. Each sample consisted of four pots with densely grown seedlings (Fig. 1), which were immediately frozen in liquid nitrogen, ground to a fine powder, and lyophilised. All mutations were verified by PCR. Mutations of PGM1, SPS and HXK1 were also validated by quantifying starch amounts as well as SPS and glucokinase activities, respectively (Supplementary Table ST1). Mutation of CHUP1 was additionally validated by microscopy (Supplementary Figure SF1).

### 2.2. Chlorophyll fluorescence measurements

Chlorophyll fluorescence parameters were recorded at ambient temperature (22 °C) with Imaging-PAM MAXI version (Heinz Walz GmbH; www.walz.com). Maximum quantum yield of PSII (Fv/Fm) was determined after 15 min of dark adaptation by supplying a saturating light pulse. Dynamics of quantum efficiency of PSII (Y(II)), electron transport rate (ETR), photochemical (qP), non-photochemical quenching (qN, NPQ), quantum yield of regulated energy dissipation (Y(NPQ)) and quantum yield of nonregulated energy dissipation (Y(NO)) were determined after 15 min of light adaption to either (i) 100 µmol $m^{-2}$ $s^{-1}$ for non-acclimated plants; or (ii) 250 µmol $m^{-2}$ $s^{-1}$ for LT/EL-acclimated plants.

### 2.3. Pigment extraction and quantification

Chlorophyll was extracted by solubilising dried plant material in 80 % acetone before samples were incubated on ice for 10 min. Following a short centrifugation at 4 °C, absorbance at 652 nm was determined in the supernatant and chlorophyll content was calculated as described earlier (Bruinsma, 1961).

Anthocyanins were quantified photometrically as described before (Kitashova et al., 2023). Lyophilized plant material was incubated with 1 M HCl at 25° C for 30 min. The samples were then centrifuged at 20, 000g, and the supernatants were transferred to a new tube. A second extraction was performed at 80° C. After centrifugation, the two supernatants were pooled, and the absorbance was measured at 540 nm. Total anthocyanin concentration was normalised to pelargonidin (C15) standards.

### 2.4. Quantification of protein amounts

Total protein amount was determined photometrically as described earlier with slight modifications (Fürtauer et al., 2018). In brief, lyophilised plant material was solubilised in 8.8 M urea and 50 mM HEPES, pH 7.8. After filtering out plant material debris, proteins were precipitated using 100 % ice cold acetone with 2 mM DTT. Pellets were washed twice with methanol and acetone, and solubilised in 8.8 M urea, 50 mM HEPES, pH 7.8. Protein amounts were quantified using the Bradford solution for protein determination (PanReac AppliChem, www.itwreagents.com).

### 2.5. Quantification of starch, soluble carbohydrates and hexose phosphates

Transitory starch, soluble carbohydrates, and hexose phosphate amounts were determined as described before (Kitashova et al. 2023). Dried plant material was incubated with 80 % ethanol at 80 °C for 30 min. Following brief centrifugation, the supernatant containing soluble sugars was transferred to a new tube. Starch-containing pellets were incubated with 0.5 N NaOH at 95 °C for 60 min before acidification with 1 M $CH_3COOH$, and then digested with amyloglucosidase, yielding glucose moieties. Glucose concentration was quantified photometrically in a glucose oxidase/peroxidase/dianisidine reaction at 540 nm.

Soluble sugar-containing ethanol extracts were dried and resolubilised in water. After incubation of samples with 30 % KOH at 95 °C, sucrose amount was quantified following an incubation with 0.14 % (w/v) anthrone in 14.6 M $H_2SO_4$ at 40 °C for 30 min, with absorbance detection at 620 nm. Glucose was quantified using a coupled hexokinase/glucose-6-phosphate dehydrogenase (G6PDH) assay, and fructose using a coupled hexokinase/phosphoglucose isomerase/G6PDH assay, which yielded NADPH detectable at 340 nm.

Glucose 6-phosphate (G6P) and fructose 6-phosphate (F6P) were extracted using trichloroacetic acid (TCA) in diethyl ether (16 % w/v). Following washing with 16 % (w/v) TCA in 5 mM EGTA, samples were neutralised with 5 M KOH/1 M triethanolamine. Samples were incubated at 30 °C for 30 min in a buffer containing G6PDH in 1 M Tricin pH 9, 10 mM $NADP^+$ (and PGI for quantifying F6P), resulting in the production of NADPH. After the remaining $NADP^+$ was depleted by adding 0.5 M NaOH and samples were neutralised with 0.5 M HCl, G6P and F6P concentrations were determined in a cyclic reaction. Samples were supplied with G6PDH in the 1 M Tricin pH 9, 100 mM $MgCl_2$, 100 mM EDTA, 100 mM G6P buffer, before being mixed with thiazolyl blue and phenazine methosulfate. The produced formazan dye was then detected at 570 nm.

### 2.6. Quantification of enzyme activities

Activities of sucrose phosphate synthase (SPS), glucokinase (GLCK), fructokinase (FRCK), and invertase (INV) were determined under substrate saturation ($v_{max}$) as described before (Kitashova et al., 2023). For quantification of SPS maximal activity, lyophilised plant material was suspended in 50 mM HEPES pH 7.5, 10 mM $MgCl_2$, 1 mM EDTA, 2.5 mM DTT, 10 % (v/v) glycerine and 0.1 % (v/v) Triton X-100. Following centrifugation at 4 °C with 20.000 g, the supernatant was incubated for 30 min at 25 °C with 50 mM HEPES pH 7.5, 15 mM $MgCl_2$, 2.5 mM DTT, 35 mM UDP-glucose, 35 mM F6P and 140 mM G6P. After the reaction was stopped by boiling samples with 30 % KOH, the produced sucrose amounts were determined as described above.

For quantification of glucokinase (GLCK) and fructokinase (FRCK) activities, dried plant material was incubated with 50 mM Tris pH 8.0, 0.5 mM $MgCl_2$, 1 mM EDTA, 1 mM DTT and 1 % (v/v) Triton X-100, then centrifuged at 4 °C at 20.000 g. The supernatant was mixed with 100 mM HEPES pH 7.5, 10 mM $MgCl_2$, 2 mM ATP, 1 mM $NADP^+$, 0.5 U G6PDH and either 5 mM glucose for glucokinase measurement or 5 mM fructose for fructokinase measurement, and absorbance was measured at 30 °C and 340 nm.

Cytosolic (cINV) and vacuolar (vINV) invertase activities were determined following extraction on ice in a buffer containing 50 mM HEPES–KOH pH 7.5, 5 mM $MgCl_2$, 2 mM EDTA, 1 mM phenylmethylsulfonylfluoride, 1 mM DTT, 10 % (v/v) glycerine and 0.1 % (v/v) Triton X-100. Activity of cINV was determined using a reaction buffer with pH 7.5 (20 mM HEPES–KOH, 100 mM sucrose), and vINV using a reaction buffer with pH 4.7 (20 mM sodium acetate, 100 mM sucrose). After incubating the samples at 30 °C and stopping the reaction by heating samples to 95 °C, glucose moieties were photometrically determined with a coupled glucose oxidase/peroxidase/dianisidine reaction at 540 nm.

### 2.7. Subcellular quantification of hexose phosphates amounts

G6P and F6P concentrations in plastids and cytosol were determined

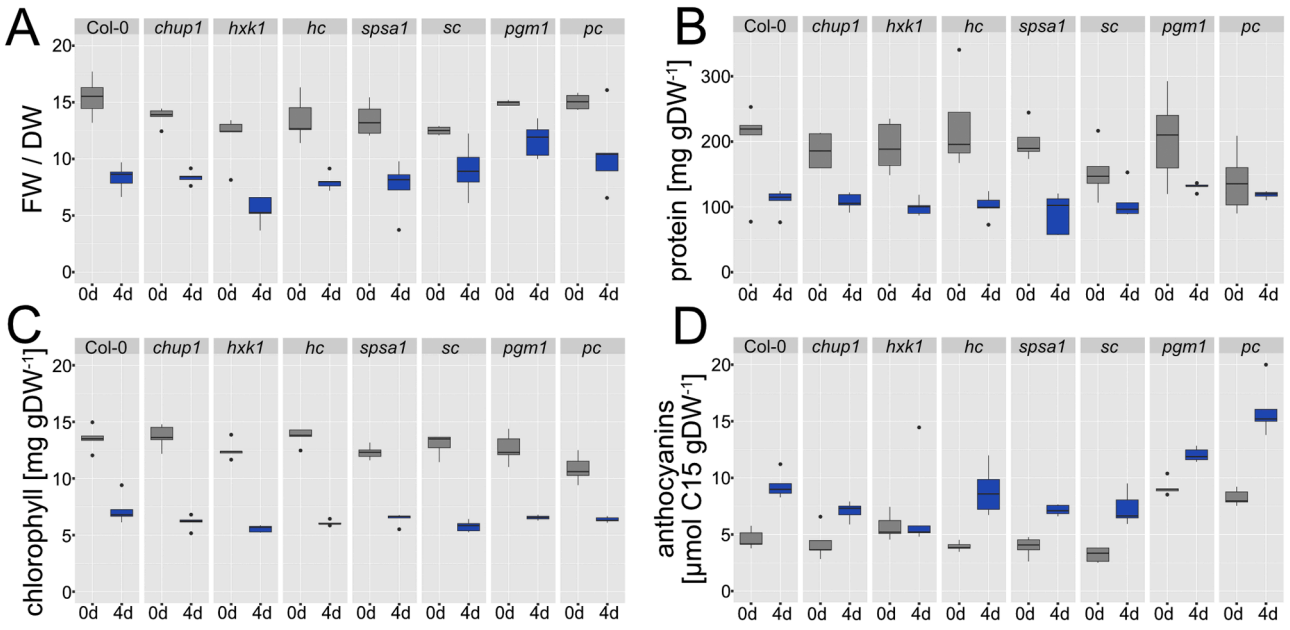


**Fig. 2.** Effects of low temperature / elevated light on biomass, proteins and pigment content in Col-0, *chup1, hxk1, hc (hxk1 x chup1), spsa1, sc (spsa1 x chup1), pgm1, pc (pgm1 x chup1)* before and after 4 days of treatment (LT/EL). (A) Ratios of fresh weight (FW) to dry weight (DW). Treatment had a significant effect in all genotypes (ANOVA, $p < 0.05$). (B) Total protein amounts normalised to dry weight. Treatment had a significant effect in all genotypes except for *pgm1* and *pc* (ANOVA, $p < 0.01$). (C) Chlorophyll content normalised to dry weight. Treatment had a significant effect in all genotypes (ANOVA, $p < 0.001$). (D) Anthocyanin content normalised to a C15 standard (pelargonidin) and to dry weight. Treatment resulted in a significant increase of anthocyanins across all genotypes except for *hxk1* (ANOVA, $p < 0.001$). $n = 5$, where each sample consisted of four pots. Grey boxes: control, i.e., 0d of LT/EL. Blue boxes: treatment, i.e., 4d of LT/EL. The full data set is provided in the supplements (Supplementary Table ST1).

by combining non-aqueous fractionation (NAF) and photometrical determination of hexose phosphates. A benchtop protocol was applied for NAF (Fürtauer et al., 2016) and adapted as described previously (Kitashova et al., 2024). In summary, lyophilised plant material was homogenised in tetrachloroethylene ($\rho = 1.60$ g cm$^{-3}$) with an ultrasonic homogenizer (Hielscher Ultrasonics UP200 St, www.hielscher.com). Following centrifugation at 20,000 g, the supernatant and pellet were separated, and the density of the supernatant was decreased using heptane ($\rho = 0.68$ g cm$^{-3}$). The supernatant was sonicated again, and after centrifugation, the pellet and supernatant were separated again. The procedure was repeated for, in total, 6 fractions with densities between 1.35 and 1.60 g cm$^{-3}$. The pellets were resuspended, split into 2 sub-fractions, and dried in a desiccator. These samples were used for (i) marker enzyme quantification; and (ii) hexose phosphate quantification. Activities of the marker enzymes alkaline pyrophosphatase (plastidial) and uridine 5′-diphosphoglucose pyrophosphorylase (cytosolic), were determined photometrically (Fürtauer et al., 2016). Subcellular hexose phosphate amounts were quantified as described above and correlated with marker enzyme activities to reveal an estimate of plastidial and cytosolic F6P and G6P proportions.

### 2.8. Transmission electron microscopy (TEM)

Seedlings were covered with aluminium foil at the end of the night prior to chemical fixation to minimize starch accumulation. Seedlings were then cut into 1 × 1 mm pieces and fixed with a buffer containing 2.5 % glutaraldehyde, 75 mM cacodylate, 2 mM $MgCl_2$, pH 7.0. The fixation process further contained washing steps with 1 % osmium tetroxide and dehydration steps with en-bloc contrasting containing 1 % uranyl acetate. For embedding, leaf pieces were polymerized in Spurr's resin of medium rigidity over night at 63 °C. Ultrathin sections of 70 nm were post stained for 2 min with lead citrate and TEM was performed with the Zeiss EM 912, outfitted with an omega filter and lanthanum hexaboride source. The Zeiss EM 912 operated at 80 kV in zero-loss mode. Images were acquired using a 2k x 2k slow-scan CCD camera (Tröndle Restlichtverstärkersysteme, Moorenweis, Germany).

### 2.9. RNA sequencing and data analysis

Total RNA from plants was isolated using Trizol (Invitrogen, Carlsbad, USA) and purified using Direct-zol™ RNA MiniPrep Plus columns (Zymo Research, Irvine, USA) according to the manufacturer's instructions. RNA integrity and quality was assessed with an Agilent 2100 Bioanalyzer (Agilent, Santa Clara, USA). Depletion of ribosomal RNA, generation of directional lncRNA-Seq libraries and 150-bp paired-end sequencing (depth of approximately 6 G) on an Illumina Novaseq 6000 system (Illumina, San Diego, USA) was conducted at Biomarker Technologies (BMK) GmbH (Münster, Germany) with standard Illumina protocols. Three independent biological replicates were used per genotype.

RNA-Seq reads were analyzed on the Galaxy platform (Jalili et al., 2020) essentially as described (Tang et al., 2024) with one exception: DESeq2 (Love et al., 2014) with the fit type set to "parametric", "multi-mapping allowed", a linear two-fold change cutoff, and an adjusted $P < 0.05$, was used to determine the differential expression of both plastid- and nuclear-encoded genes.

### 2.10. Data analysis and statistics

Data was evaluated and statistically analysed using RStudio (Posit Team, 2024) and MATLAB® (www.mathworks.com). Prior to analysis of variance, statistical outliers of each variable were replaced by medians or mean values. If sample sizes varied within one data table, e.g., between hexose phosphates ($n = 6$) and soluble sugars/enzyme activities ($n = 5$), missing values were filled by mean values. GO term enrichment analysis was performed using PlantRegMap with a threshold p-value ≤ 0.001 (Tian et al., 2020).

Protein-protein docking was performed using ClusPro 2.0 (https://cluspro.org/). ClusPro docking is comprised of a multi-step process including analysis of approx. 70,000 rotations, followed by clustering of

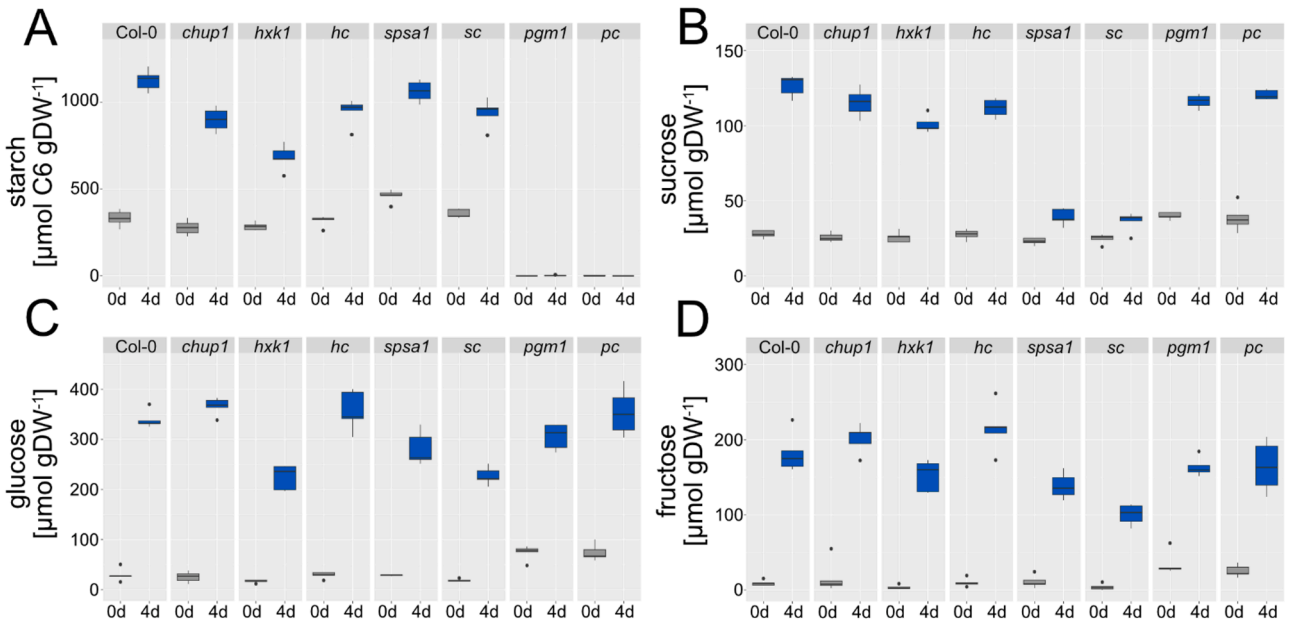


**Fig. 3.** Carbohydrate changes under low temperature and elevated light in Col-0, *chup1, hxk1, hc (hxk1 x chup1), spsa1, sc (spsa1 x chup1), pgm1, pc (pgm1 x chup1)* before and after 4 days of low temperature / elevated light (LT/EL). (A) Starch amounts in C6 equivalents. Treatment of 4d LT/EL resulted in a significant increase across all genotypes except for *pgm1* and *pc* (ANOVA, $p < 0.001$). (B) Sucrose amounts before (0d) and after (4d) treatment. Amounts significantly increased in all genotypes due to LT/EL (ANOVA, $p < 0.01$). (C) Glucose amounts before (0d) and after (4d) treatment. Amounts significantly increased in all genotypes due to LT/EL (ANOVA, $p < 0.001$). (D) Fructose amounts before (0d) and after (4d) treatment. Amounts significantly increased in all genotypes due to LT/EL (ANOVA, $p < 0.001$). $n = 5$. Grey boxes: control, i.e., 0d of LT/EL. Blue boxes: treatment, i.e., 4d of LT/EL. The full data set is provided in the supplements (Supplementary Table ST1).

the resulting models based on structural similarity, before refining the top-scoring models. Finally, the docking algorithm considered several energy terms, including van der Waals attractive and repulsive forces, electrostatic interactions, and desolvation contributions, to generate a balanced scoring function for ranking models (Kozakov et al., 2017).

All data is provided in a repository (https://git.nfdi4plants.org/thomas.naegele/Bagshaw_et_al_HXK1_CHUP1).

## 3. Results

### 3.1. Seedlings of hxk1 are affected in growth and leaf metabolism under combined cold and elevated light

To reveal a potential regulatory interaction between cold and elevated light-induced changes in chloroplast positioning and central carbohydrate metabolism, wild type plants of the *A. thaliana* accession Col-0, and seven mutants with deficiencies in chloroplast movement (*chup1*), starch biosynthesis (*pgm1*), sucrose biosynthesis (*spsa1*), or glucose phosphorylation and sugar signalling (*hxk1*), as well as the double mutants *pgm1* x *chup1* (*pc*), *spsa1* x *chup1* (*sc*), and *hxk1* x *chup1* (*hc*) were analysed before and after 4 days of exposure to a combination of low temperature and elevated light intensities (LT/EL). After 4 days of LT/EL, a growth phenotype with pale leaf areas was observed in *hxk1* (Fig. 1B). Interestingly, the phenotype of *hxk1* plants was suppressed by the additional mutation of *chup1* in the *hc* double mutant (Fig. 1F). Plants of the *pgm1* and *pc* mutants were the smallest among all genotypes (Fig. 1C, G). The growth experiment was repeated, and all phenotypes could be reproduced under these conditions.

The treatment of LT/EL significantly reduced the ratio of fresh weight (FW) to dry weight (DW) in all genotypes (Fig. 2A). The highest median was observed in the wild type under control conditions (0d) which showed a >15-fold higher FW than DW. Lowest medians at 0d were observed for *hxk1* and *sc* which was an approx. 12.5-fold higher FW than DW. After 4d of LT/EL, median ratios dropped below a ratio of 10 in all genotypes except for *pgm1* and *pc,* which showed a ratio of ~12 and ~10.5, respectively. The lowest ratio was observed for *hxk1* at LT/EL (median FW/DW ~5).

Across all genotypes, the total protein amount at 0d showed a similar median value of ~200 mg $gDW^{-1}$ except for double mutants *sc* and *pc,* which had a lower content of ~150 mg $gDW^{-1}$ (Fig. 2B). After 4d at LT/EL, protein amount dropped to ~100 mg $gDW^{-1}$ and was highest in *pgm1* (~130 mg $gDW^{-1}$). The double mutant *pc* was the only genotype which did not show a significant reduction of protein amount under LT/EL.

Chlorophyll content at 0d was between 10 and 14 mg $gDW^{-1}$ and significantly dropped in all genotypes to values between 5 and 7 mg $gDW^{-1}$ after 4d LT/EL (Fig. 2C). Both mutants of *hxk1* and *sc* had a significantly lower chlorophyll content than Col-0 under LT/EL (ANOVA, $p < 0.01$).

In all genotypes, photometrically determined anthocyanin contents increased significantly after 4d LT/EL except for *hxk1,* which showed a similar median value before and after treatment (Fig. 2D). Highest amounts of anthocyanins were determined in *pgm1* and *pc* which showed approx. 1.5x-fold higher values than Col-0 under both conditions.

Carbohydrate amounts were strongly and significantly affected due to the LT/EL treatment (Fig. 3). Compared to Col-0, the *spsa1* mutant had significantly elevated starch amounts under control conditions (ANOVA, $p < 0.01$) which was not observed at LT/EL (Fig. 3A). The *hxk1* mutant was found to accumulate significantly less starch than Col-0, while in the *hc* (and also *sc*) double mutant, starch accumulated to similar amounts as in the *chup1* mutant. Treatment-induced changes of sucrose amounts were significantly affected in both *spsa1* and *sc* which showed the lowest sucrose amounts after 4d LT/EL (Fig. 3B). In *pgm1* and pc mutants, sucrose amount was significantly higher than in Col-0 before (0d), yet not after, 4d of LT/EL. Both hexoses, i.e., glucose and fructose, followed similar trends across all genotypes (Fig. 3C, D). Under control conditions, hexose amounts were highest in *pgm1* and *pc* mutants while, under LT/EL, amounts rose highest in *chup1* and *hc*.

In summary, these observations showed that, after 4d at LT/EL, seedlings of *hxk1* mutants were significantly affected in their (above-ground) phenotype, which was also reflected on the molecular level (e.g., anthocyanins, starch and sucrose amounts). Interestingly, this effect

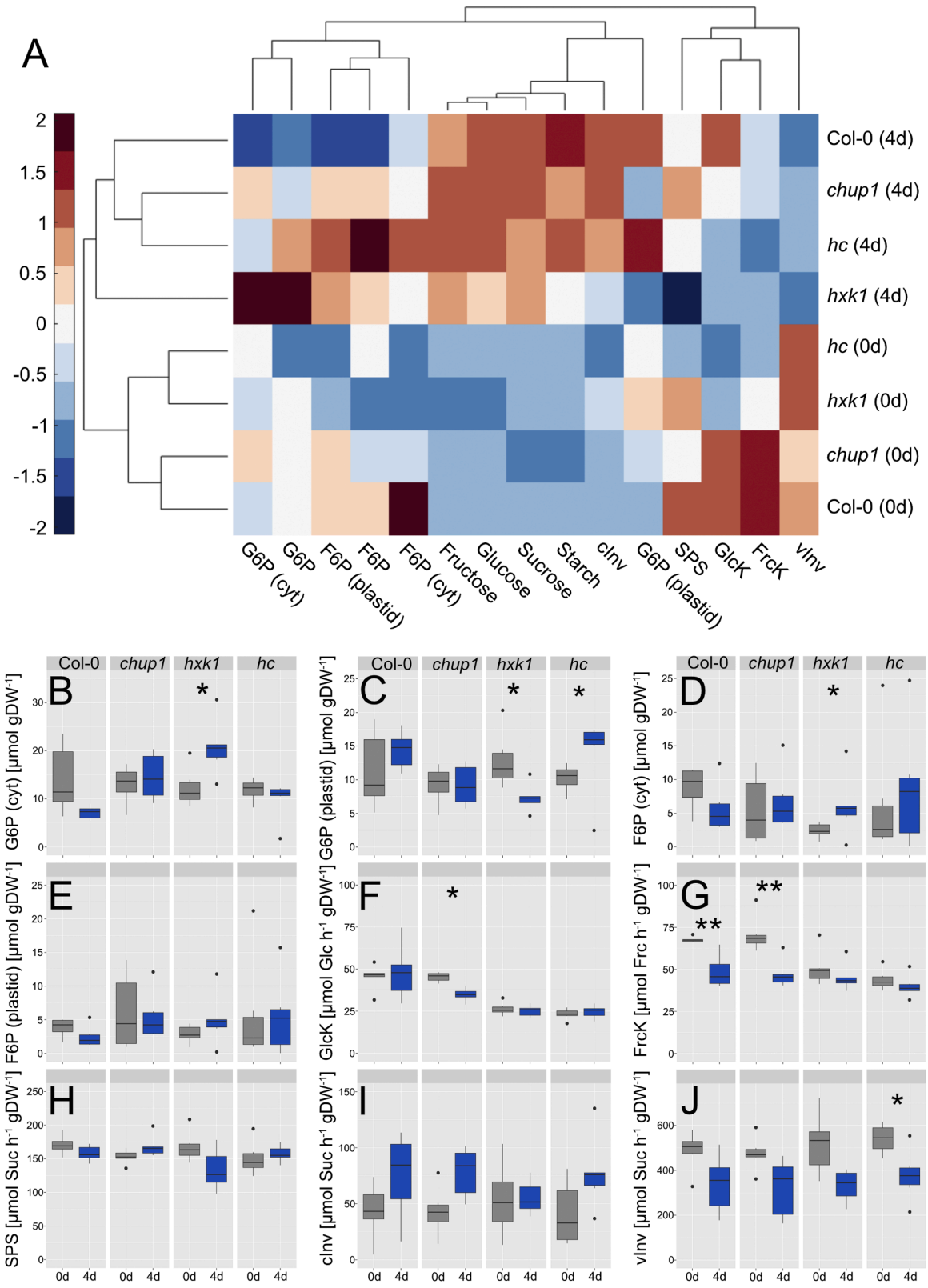


**Fig. 4.** Regulation of carbohydrate metabolism under LT/EL treatment. (A) Euclidean distance-based hierarchical clustering of the central carbohydrate metabolism between Col-0, *chup1, hxk1* and *hc*. Trees of samples (rows) and variables (columns) were derived from Euclidean distances of medians for each variable ($n = 5$–6). Medians were z-scaled (i.e., zero mean/unit variance), and scaled values are presented by the colorbar. (B) Amounts of cytosolic G6P, (C) Amounts of plastidial G6P, (D) Amounts of cytosolic F6P, (E) Amounts of plastidial F6P, (F) Activity ($v_{max}$) of GlcK, (G) Activity ($v_{max}$) of FrcK, (H) Activity ($v_{max}$) of SPS, (I) Activity ($v_{max}$) of cInv, (J) Activity ($v_{max}$) of vInv in Col-0, *chup1, hxk1*, and *hc (hxk1 x chup1)*, before and after 4 days of low temperature / elevated light (LT/EL). Grey boxes: control conditions (0d), blue boxes: 4d LT/EL (4d). Asterisks indicate significance (* $p < 0.05$, ** $p < 0.01$, ANOVA/Tukey HSD posthoc test). G6P: glucose 6-phosphate; F6P: fructose 6-phosphate; cInv: cytosolic invertase; vInv: vacuolar invertase; SPS: sucrose phosphate synthase; GlcK: glucokinase; FrcK: fructokinase; cyt: cytosolic. The full data set is provided in the supplements (Supplementary Table ST1).

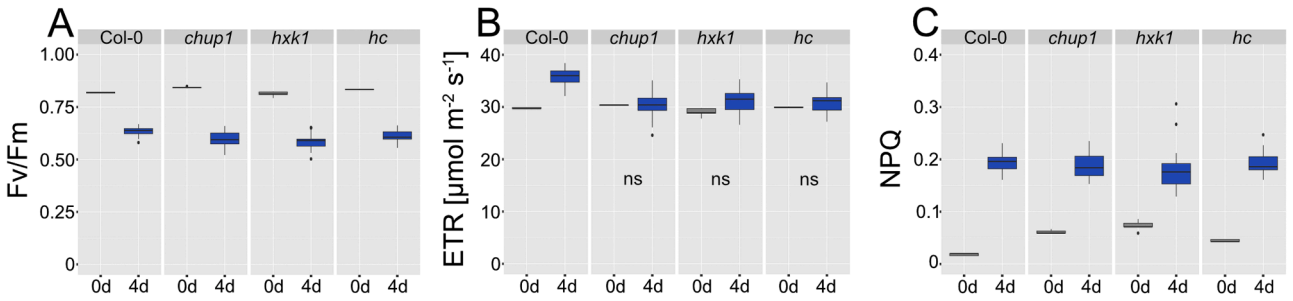


**Fig. 5.** Chlorophyll fluorescence analysis in Col-0, *chup1, hxk1*, and *hc (hxk1 x chup1)* before and after 4 days of low temperature / elevated light (LT/EL). (A) Maximum quantum yield of Photosystem II (Fv/Fm); (B) linear electron transport rates (ETR); (C) non-photochemical quenching (NPQ). Parameters were determined at 22 °C and growth PAR intensity, i.e., at 100 µmol photons $m^{-2}$ $s^{-1}$ for control plants and at 250 µmol photons $m^{-2}$ $s^{-1}$ for LT/EL plants. Values of control (0d) and treatment (4d) differed significantly (ANOVA, $p < 0.001$) within each genotype except for comparisons labelled with 'ns' (not significant). Grey boxes: control (0d), blue boxes: LT/EL treatment (4d). $n = 5$. An overview of all data is provided in the supplements (Supplementary Table ST1).

was suppressed both on a phenotypic and metabolic level in the double mutant *hc*, i.e., when, in addition to HXK1, also CHUP1 was deficient. This suppression was neither observed in *sc* nor in *pc* double mutants, indicating a specific effect between CHUP1 and HXK1 rather than a general effect of (metabolic) acclimation.

### 3.2. Cytosolic hexose phosphate amounts increase in hxk1 under LT/EL

Hexokinase 1 (HXK1) catalyses the phosphorylation of glucose to G6P in a reaction located in the cytosol. To evaluate how this reaction was affected due to the HXK1 mutation, hexokinase activity was determined together with other central enzyme activities and the subcellular distribution of G6P and F6P between the cytosol and plastids (Fig. 4).

Under control conditions (0d), carbohydrate metabolism in Col-0 and *chup1* built one cluster while *hxk1* clustered together with *hc*. This was predominantly due to significantly higher FrcK and GlcK activities in Col-0 and *chup1* (ANOVA, $p < 0.05$), whereas vInv activities were higher in *hxk1* and *hc*. After 4d of LT/EL, *chup1* and *hc* clustered together, while *hxk1* differed most from all other genotypes. The total G6P amount and its cytosolic fraction were most elevated in *hxk1* under these conditions while the plastidial G6P fraction was lower than in Col-0, *chup1* and *hc*. Also, SPS activity was found to be lower in *hxk1* than in the other genotypes.

The most significant effects, which separated *hxk1* from all other genotypes under LT/EL, were (i) increased amounts of cytosolic G6P and F6P, and (ii) decreased G6P amounts in the plastid (Fig. 4B, C, D). In the double mutant *hc*, cytosolic amounts of G6P and F6P did not differ significantly between 0d and 4d, which reflected the changes in Col-0 and *chup1* (Fig. 4B, D). Plastidial G6P significantly increased in *hc* under LT/EL (Fig. 4C).

Chlorophyll fluorescence analyses were conducted to evaluate if the

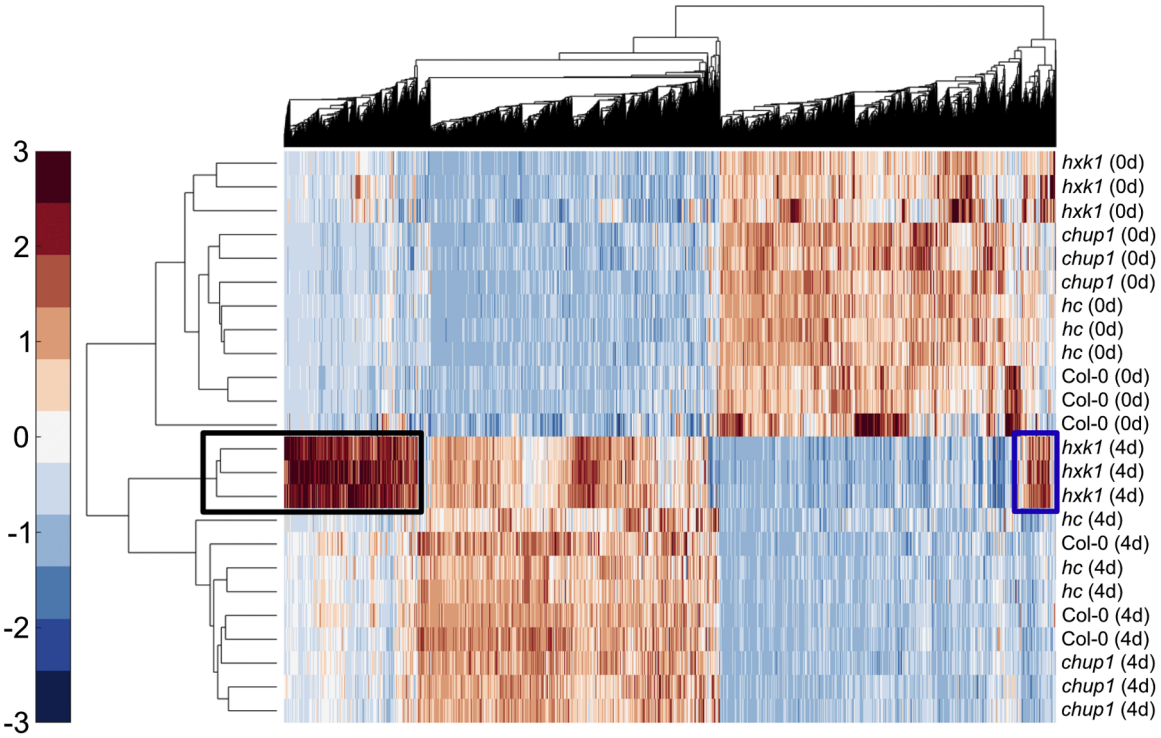


**Fig. 6.** Hierarchical clustering of transcripts and samples in Col-0, *chup1, hxk1*, and *hc (hxk1 x chup1)* before and after 4 days of low temperature / elevated light (LT/EL). Only transcripts were considered which were, at least, significantly different between conditions or two genotypes (ANOVA, $p < 0.001$). Each row represents a sample (labels on the right side). Each column represents a candidate gene. Trees were derived from Euclidean distances. The colorbar indicates z-scaled normalised expression values (i.e., zero mean – unit variance scaling). Black box: candidate genes which were only upregulated under LT/EL in *hxk1*. Blue box: constitutively upregulated candidate genes in *hxk1* under LT/EL. Lists of candidate genes are provided in the supplements (Supplementary Tables ST3 and ST4).

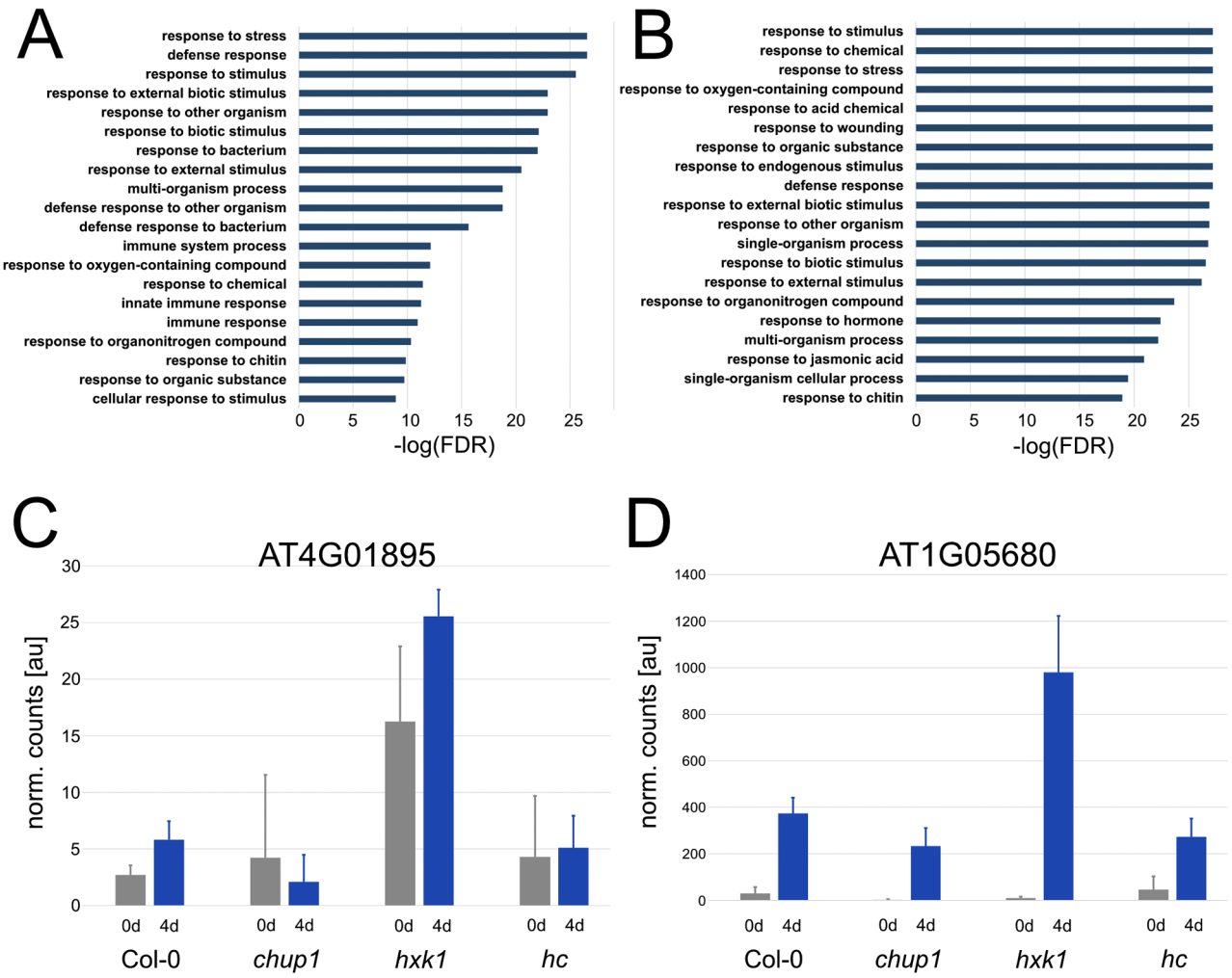


**Fig. 7.** GO term enrichment analysis of upregulated genes in *hxk1*. (A) List of the 20 most significantly enriched GO terms among constitutively upregulated transcripts in *hxk1* (corresponds to the blue box in Fig. 6; Supplementary Table ST4). (B) List of the 20 most significantly enriched GO terms among upregulated transcripts in *hxk1* under LT/EL (corresponds to black box in Fig. 6; Supplementary Table ST4). Full lists of significantly enriched terms are provided in the supplements (Supplementary Table ST5). (C) Transcript levels of the Systemic Acquired Resistance (SAR) regulator protein NIMIN-1-like protein (AT4G01895), before (0d) and after (4d) LT/EL. (D) Transcript levels of Uridine Diphosphate Glycosyltransferase 74E2 (AT1G05680), before (0d) and after (4d) LT/EL. Bars represent means +/- SD, $n = 3$.

observed differences in carbohydrate metabolism were potentially due to, or related to, differential photosynthetic efficiencies. Analyses were only performed on obviously green leaf tissue, i.e., pale/faded leaf area in *hxk1* under LT/EL was excluded from the analysis. Maximum quantum yield of Photosystem II (Fv/Fm) was determined from dark adapted leaves and was found to significantly decrease due to 4d LT/EL in all genotypes (Fig. 5A). At 4d LT/EL, *hxk1* had a slightly, but significant, lower Fv/Fm than Col-0.

Comparison of linear electron transport rates (ETR), which were determined after exposure of leaf tissue to growth light intensity, revealed a significant treatment effect only in Col-0 (ANOVA, $p < 0.001$, Fig. 5B). Non-photochemical quenching (NPQ) significantly increased due to treatment and reached similar values in all genotypes after 4d at LT/EL (ANOVA, $p < 0.001$, Fig. 5C). Interestingly, under control conditions, all mutants had significantly higher NPQ values than Col-0, and *hxk1* had the highest median value of ~0.75 (Fig. 5C).

### 3.3. Deficiency of HXK1 induces an immune response of the transcriptome

Transcript levels were quantified to evaluate how deficiencies of CHUP1, HXK1, or both affect leaf tissue response to LT/EL. In total, ~32,500 transcribed genes were detected in at least one sample (Supplementary Table ST2). To reveal the most significant effects, transcripts were selected which significantly differed between at least two genotypes or control and treatment, respectively ($p < 0.001$, ANOVA and TukeyHSD posthoc test incl. correction for multiple testing). This resulted in the identification of 10,094 candidate genes (Supplementary Table ST3). A hierarchical cluster analysis of these significantly affected candidates revealed a group of 1742 candidate genes of which transcripts were significantly upregulated only in *hxk1* mutants after 4d LT/EL (Fig. 6, black box). Another cluster of 441 candidate genes was detected which were constitutively upregulated in *hxk1* compared to all other genotypes (Fig. 6, blue box). Lists of candidate genes in both clusters are provided in the supplement (Supplementary Table ST 4).

As expected, both *HXK1* and *CHUP1* were among the significantly affected transcripts (Supplementary Figure SF3 A, B). The transcript levels of *HXK1* did not vary significantly in *hxk1* under LT/EL while *CHUP1* transcript levels significantly decreased due to treatment, also in the *chup1* and *hc* mutants. Transcript levels of *PGM1*, which catalyses a central step in starch biosynthesis, strongly and significantly decreased in *hxk1* under LT/EL (Supplementary Figure SF3 D). While transcript amounts of chalcone synthase, which catalyses the first committed step of flavonoid/anthocyanin biosynthesis, significantly increased in all

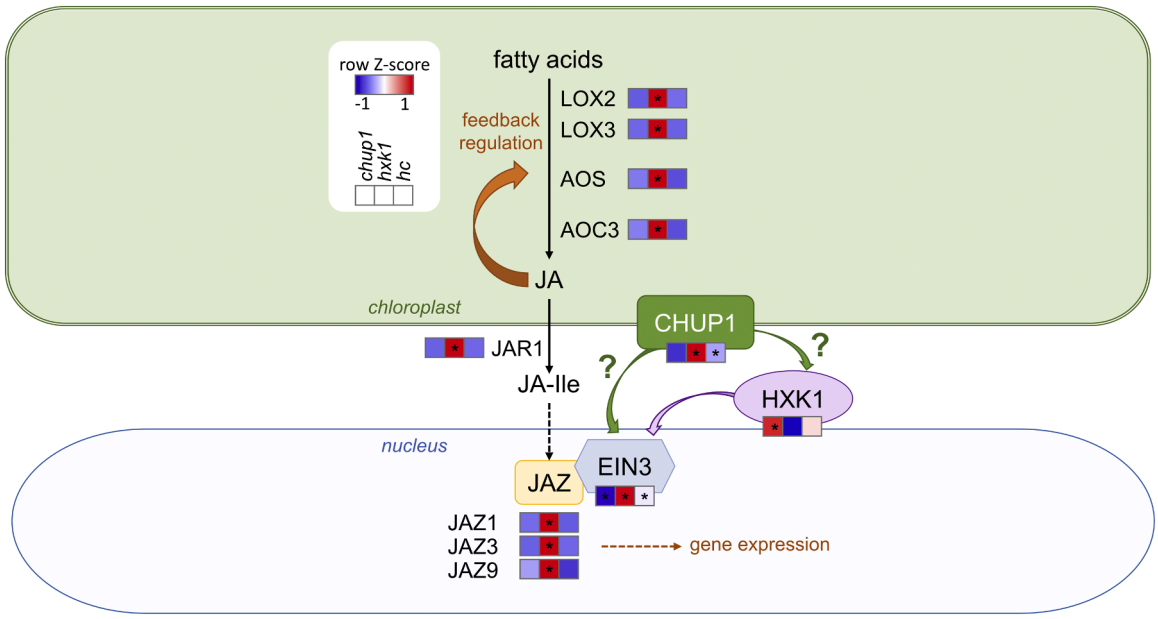


**Fig. 8.** A putative transcriptional regulation of jasmonic acid biosynthesis and signaling pathways by CHUP1 and HXK1. Color boxes beside and below indicated proteins represent mean fold change of transcripts of *chup1* (left box), *hxk1* (middle box) and *hc* (right box; *hxk1 x chup1*) relative to that of Col-0. Transcript levels of *chup1, hxk1*, and *hc* were normalized to those of Col-0 for each time point respectively before calculating the fold increase between 4D and 0D of treatment (LT/EL). Asterisks represent significance (ANOVA, $p < 0.01$). $n = 3$. Abbreviations: AOC3 - ALLENE OXIDE CYCLASE 3, AOS - ALLENE OXIDE SYNTHASE, CHUP1 - CHLOROPLAST UNUSUAL POSITIONING 1, EIN3 - ETHYLENE-INSENSITIVE3, HXK1 – HEXOKINASE1, JA - Jasmonic acid, JA-Ile – Jasmonic acid isoleucine, JAR1 - JASMONATE RESISTANT 1, JAZ1 -JASMONATE-ZIM-DOMAIN PROTEIN 1, JAZ3 - JASMONATE-ZIM-DOMAIN PROTEIN 3, JAZ9 - JASMONATE-ZIM-DOMAIN PROTEIN 9, LOX2 - LIPOXYGENASE 2, LOX3 - LIPOXYGENASE 3.

genotypes under LT/EL, the transcript levels in *hxk1* only increased to ~30 % of the other genotypes (Supplementary Figure SF3 F).

A Gene Ontology (GO) term enrichment analysis showed that genes, which were either constitutively upregulated (Fig. 7A) or upregulated under LT/EL (Fig. 7B) in *hxk1*, belonged to the significantly enriched terms of 'stress response', 'defense response', as well as response to 'stimulus', 'biotic stimulus' or 'wounding'. This significantly differed from enrichments in all other genotypes (Supplementary Figure SF4, Supplementary Table ST5). As an example for the *hxk1*-specific stress response, transcripts of the *Systemic Acquired Resistance (SAR) regulator protein NIMIN-1-like protein* (AT4G01895) were constitutively elevated in *hxk1* than in other genotypes (Fig. 7C). Additionally, transcript levels of *Uridine Diphosphate Glycosyltransferase 74E2* (AT1G05680) were induced by LT/EL across all genotypes, but the response effect was strongest in *hxk1* (Fig. 7D).

Further significantly enriched terms were 'innate immune response', 'immune response', and 'response to jasmonic acid'. Two central regulators of jasmonate signalling pathways, Jasmonic acid-amino synthetase (*JAR1*, AT2G46370) and *JAZ* (jasmonate-ZIM domain proteins) transcripts were prominently represented in the 'response to jasmonic acid' GO term. JAR1 is a key enzyme in plant hormone biosynthesis, catalysing the conjugation of jasmonic acid with amino acids, namely isoleucine, to regulate plant biotic stress responses. Acting downstream from JAR1, JAZ proteins are key transcriptional regulators, repressing transcription of jasmonate-responsive genes (Ruan et al., 2019). Only in the *hxk1* mutant both transcripts of *JAR1* and *JAZ* were significantly over-represented after 4 days of LT/EL exposure (Fig. 8).

Previous studies demonstrated that ethylene-stabilised transcription factors (EIN3) directly interact with JAZ1, JAZ3 and JAZ9 proteins to mediate jasmonate signalling (Zhu et al., 2011). Additionally, EIN3 degradation relays on HXK1-mediated glucose signalling (Yanagisawa et al., 2003). *EIN3* transcript levels showed contrasting patterns across the mutants: decreased abundance was observed in *chup1*, increased abundance in *hxk1*, and intermediate levels in the *hc* double mutant (Fig. 8).

In spinach, HXK1 was shown to associate with the chloroplast membrane (Wiese et al., 1999). Assuming that CHUP1 is localised to the chloroplast membrane, a potential interaction between HXK1 and CHUP1 in *A. thaliana* was investigated. *In silico* protein-protein docking revealed a potential non-covalent binding between the two proteins (Supplementary Figure SF2, Supplementary Model SM1). From the generated models, the one with the largest cluster size, indicating least variable interaction positions, and the lowest energy score was further analyzed. This model had a cluster size of 78 members and a centre energy of −1163.3 arbitrary units (for comparison: a previously published ClusPro protocol demonstrated a cluster size of 253 members with an energy score of −739.1 for an experimentally validated strong interaction (Kozakov et al., 2017)). While the number of cluster members was smaller in the present study, the negative energy score (−1163.3) suggested a potential interaction between CHUP1 and HXK1.

In summary, together with the enrichment analysis, these observations suggested HXK1 to be involved in the regulation of transcriptional regulation of plant immune response. This response probably depends on CHUP1, particularly under combined LT/HL exposure.

## 4. Discussion

### 4.1. Carbohydrate metabolism is highly plastic under LT/EL

Plant responses to dynamic environmental conditions are multifaceted and depend on a tightly regulated molecular network which coordinates environmental perception with metabolic and signalling responses (Ding et al., 2020). Stabilizing photosynthetic $CO_2$ uptake under stressful conditions is of utmost importance for plants to be able to acclimate, grow and propagate in a changing environment. Photosynthetic efficiency and $CO_2$ assimilation rates depend, among others, on positioning of chloroplasts and regulation of carbohydrate metabolism (Gotoh et al., 2018; Kitashova et al., 2021; Seydel et al., 2022). Particularly, under stress combinations like low temperature and high light, plants need to efficiently regulate photosynthetic activity with

carbohydrate biosynthesis to prevent limitations in electron transport, ATP biosynthesis and/or redox metabolism (Geigenberger et al., 2017; Kleine et al., 2021; Schwenkert et al., 2022). In the present study, both cell biological and metabolic functions and pathways were mutated to reveal their roles in stabilising photosynthesis in a LT/EL regime. A deficiency of SPS activity resulted in a strongly affected sucrose accumulation response under LT/EL in both *spsa1* and *sc* mutants. This suggests that affected chloroplast positioning due to CHUP1 deficiency does not amplify nor release the limitation of sucrose biosynthesis in a *spsa1* background. This indicates that metabolite transport across the chloroplast envelope, e.g., catalysed by the triose phosphate/ phosphate translocator for triose phosphate supply in the cytosol, seems not to be permanently affected by the spatially dense accumulation of chloroplasts (see Supplementary Fig. SF1). A mutation of *PGM1* resulted in significantly elevated sugar amounts under control conditions, which indicates the shift of carbon partitioning from starch biosynthesis to sucrose biosynthesis and other anabolic pathways (Gibon et al., 2009; Brauner et al., 2014). However, as already observed for *spsa1*, additional CHUP1-deficiency did not significantly affect the carbohydrate amounts of *pgm1*, neither under control nor under stress conditions. Hence, in addition to the cytosolic sucrose biosynthesis pathway, the chloroplast-located pathways of carbohydrate metabolism also did not seem to be significantly affected under analysed conditions by the polar chloroplast accumulation in the cells. In summary, these findings indicate a high plasticity of photosynthesis and carbohydrate metabolism under LT/EL that is stabilized even with affected localization of photosynthetic organelles, which has been shown to have significant impact on biomass accumulation (Gotoh et al., 2018).

### 4.2. Transcript analysis suggests increased susceptibility of the hxk1 mutant for biotic stress under LT/EL

In contrast to *spsa1* and *pgm1* mutants, the *hxk1* mutant did not accumulate (photometrically measurable) anthocyanins under LT/EL (see Fig. 2D). This is in line with a previous study which demonstrated that apple hexokinase MdHXK1 was involved in glucose sensing and regulation of anthocyanin biosynthesis (Hu et al., 2016). Also, a decrease of plastidial G6P in *hxk1* after 4 days LT/EL may indirectly indicate metabolic precursor limitation for flavonoid biosynthesis (Maeda and Dudareva, 2012). Finally, the finding of a reduced expression of *CHS* in *hxk1* (see Fig. 1 and Supplementary Figure SF3 F) further supports the hypothesis of a repression of flavonoid accumulation by microbe-associated molecular patterns triggered immunity (Serrano et al., 2012).

Under LT/EL, the *hxk1* mutant had a lower ratio of fresh weight to dry weight, significantly lowered chlorophyll content and less starch, sucrose and glucose than Col-0 (see Fig.2A, C and Fig. 3A, B, C). Together with the growth phenotype, which showed lesions and/or pale leaf areas, this suggests a significant impact on photosynthesis and carbohydrate metabolism (see Fig. 1). The quantification of subcellular hexose phosphates revealed an overaccumulation of G6P in the cytosol of *hxk1* while the plastidial fraction was depleted under LT/EL. Together with the significantly reduced *PGM1* and *BAM3* transcripts, this suggests that reduced starch amounts in *hxk1* resulted rather from a combination of substrate depletion and downregulation of the starch biosynthesis pathway than an increased rate of starch degradation (Supplementary Figure SF3).

Surprisingly, chlorophyll fluorescence analysis of the (obviously) green leaf areas revealed only a slight, yet still significant, reduction of Fv/Fm in *hxk1* compared to Col-0. The significance of this effect was reduced in *hc* double mutants (i.e., $p > 0.05$), suggesting a stabilising effect of the *CHUP1* mutation in the *hxk1* background. In contrast, while Col-0 significantly increased ETR after 4d LT/EL, the ETRs of treated *chup1, hxk1* and *hc* mutants did not differ from those of the control. This missing acclimation of photosynthetic electron transport might have different causes: in *chup1* a missing relocation of chloroplasts probably limits the efficiency of photochemistry (Gotoh et al., 2018), while in *hxk1* it might be that the observed reduction of carbon partitioning into starch and other metabolic pathways feedback inhibits and/or limits the rate of electron transport. Although overexpressing, and not attenuating, HXK1 has been found to inhibit photosynthesis (Dai et al., 1999; Granot et al., 2014), it might be that due to the combined LT/EL stress condition, other effects or regulatory factors caused a limitation or repression of photosynthetic acclimation. In this context, the analysis of the transcriptome revealed a strong and highly significant enrichment of transcripts which belong to biotic stress and immune response categories in *hxk1* under LT/EL. Among these transcripts, also central regulators of the jasmonic acid biosynthesis and signalling pathways were found, i.e. *JAR1* and *JAZ*, as well as *13-LOX, AOS, AOC*, (see Fig. 8). Based on previous findings which suggested HXK1 to be a positive regulator of plant immunity (Jing et al., 2020), this indicates that *hxk1* is susceptible to fungal or bacterial infection which caused the strong transcriptional response. Under control conditions, such a response was already observed, but it was significantly amplified by the 4 days of LT/EL treatment. This suggests a role of HXK1 in integrating and regulating plant responses towards biotic and abiotic stressors simultaneously.

Suppression of the *hxk1* phenotype in the *hc* double mutant suggests an interference of chloroplast positioning, mediated by CHUP1, and a HXK1 function. The role of chloroplast positioning in biotic stress response has previously been explored in *Nicotiana benthamiana*, where pathogen invasion triggered chloroplast rearrangement and clustering around the nucleus (Ding et al., 2019). The authors observed that chloroplast accumulation near the nucleus is a conserved response to various biotic stress signals, including viral and bacterial infections. This response occurs rapidly, i.e., within one hour, and depends on reactive oxygen species. Notably, in *N. benthamiana*, this chloroplast clustering became more pronounced when the *CHUP1* gene was mutated (Nedo et al., 2024), potentially enhancing chloroplast-nucleus signalling through increased proximity and/ or surface interaction. Similarly, in *A. thaliana*, chloroplast positioning in the epidermis has been shown to play a crucial role in controlling the entry of fungal pathogens (Irieda and Takano, 2021). The authors showed that blocking this epidermal chloroplast response significantly decreases preinvasive nonhost resistance of *A. thaliana* against fungi. Based on their experiments, they suggested that CHUP1 is a negative regulator of the epidermal chloroplast response. Chloroplast relocation is typically induced by light or cold stress (Kodama et al., 2008; Tanaka et al., 2017), and the suppression of the *hxk1* phenotype in the *hc* double mutant further suggests that the chloroplast positioning plays a crucial regulatory role in integrating metabolic signals under environmental stress. One possible explanation for the synergistic effects of CHUP1 and HXK1 is their direct interaction which seems to be plausible as indicated by *in silico* molecular docking (Supplementary Figure F2, Supplementary Model M1). This interaction may facilitate chloroplast accumulation next to the nucleus, which might affect HXK1 signalling.

HXK1 has previously been found to negatively regulate EIN3 stability, which is a transcription factor that directly interacts with JAZ proteins (Yanagisawa et al., 2003; Zhu et al., 2011). *EIN3* expression was upregulated in the *hxk1* mutant but downregulated in *chup1*, while the *hc* double mutant showed an intermediate expression level (see Fig. 8). Although the interaction mechanism between CHUP1 and EIN3 remains elusive, these observations suggest a synergistic role of both CHUP1 and HXK1 in modulating EIN3, and, consequently, jasmonic acid-related signalling. Chloroplast proximity to the nucleus appears to be critical for biotic stress resilience and retrograde signalling (Nedo et al., 2024). As the formation of stromules, i.e., tubules extending from the plastid surface that are filled with stroma, is temperature dependent and decreases under low temperature conditions (Holzinger et al., 2007), exposure to LT/EL may impact the CHUP1-HXK1 relationship by interfering with the chloroplast-nucleus interaction surface (Nedo et al., 2024; Natesan et al., 2005). In this context, the absence of CHUP1 could amplify retrograde signalling due to increased chloroplast clustering

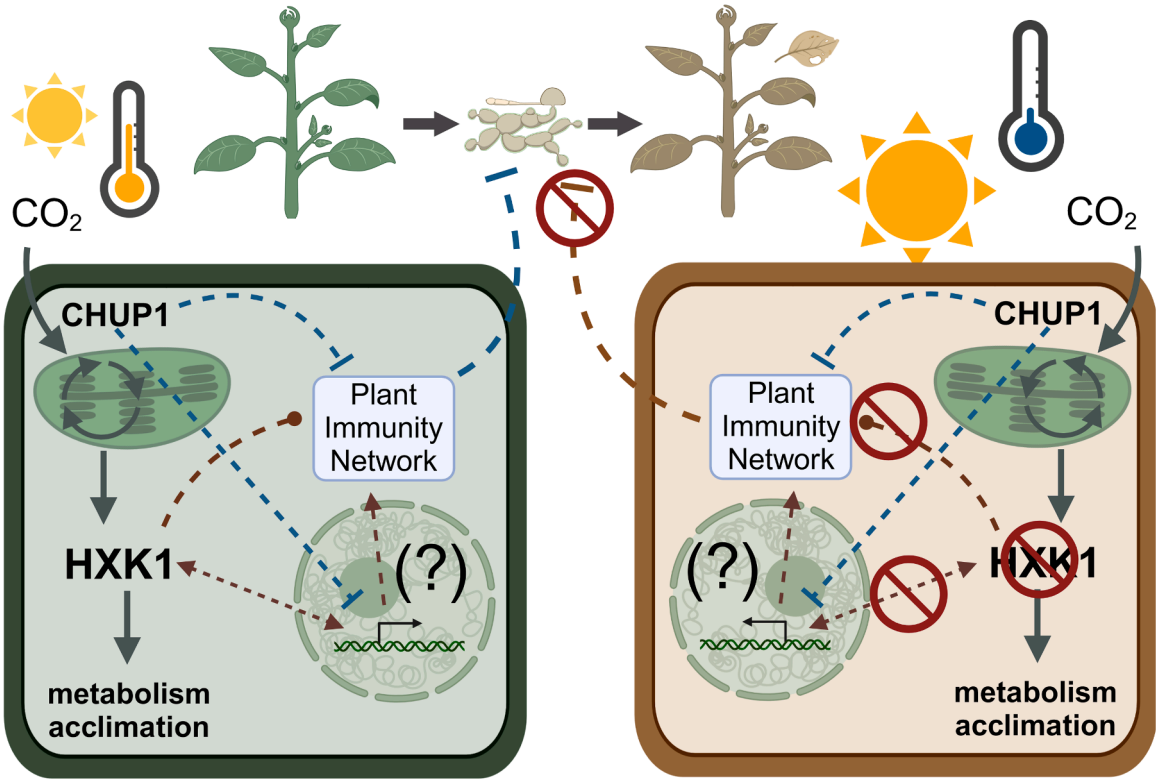


**Fig. 9.** Suggested model to connect HXK1 and CHUP1 to the plant immune network. Solid lines indicate carbon fluxes, dashed lines indicate regulatory interactions. CHUP1 acts as a negative regulator of plant immunity and HXK1 as a positive regulator. Simultaneously, both have a function in photosynthesis, metabolic regulation and acclimation to a changing environment. In *hxk1* mutants, CHUP1 negatively affects plant immunity which makes the plants more susceptible to biotic stress. This is amplified by abiotic stress, e.g., LT/EL. Left side: wild type model, right side: model for *hxk1* plants under LT/EL. Created in https://BioRender.com.

around the nucleus, likely enhancing the jasmonic acid response. Conversely, absence of HXK1 may impair EIN3 stability, affecting JAZ protein stability and therefore weakening pathogen response. The suppression of a *hxk1* phenotype in the *hc* double mutant then would have probably resulted from the compensatory effect of CHUP1 deficiency, where the absence of the positive immune regulator HXK1 is counterbalanced by the loss of the negative regulator CHUP1 (Fig. 9). In summary, these findings suggest that CHUP1 and HXK1 act as positional and metabolic regulators of signalling under environmental changes, synergistically modulating metabolic reprogramming under low temperature and elevated light conditions.

These findings clearly indicate that photosynthesis, the carbohydrate metabolism and the response toward biotic and abiotic stressors are integrated in a regulatory and signalling network in which HXK1 plays a central role. Finally, due to the observation that *chup1* rescued the *hxk1* phenotype, knocking out or down CHUP1 might represent a (conserved) strategy to improve plant immunity which needs to be evaluated in future studies.

## CRediT authorship contribution statement

**Sophia Bianca Bagshaw:** Writing – review & editing, Writing – original draft, Investigation, Formal analysis, Data curation. **Anastasia Kitashova:** Writing – original draft, Formal analysis, Data curation. **Beyza Özmen:** Data curation. **Chun Kwan Yip:** Data curation. **Bianca Emily Süling:** Data curation. **Laura Schröder:** Data curation. **Tatjana Kleine:** Formal analysis, Data curation. **Thomas Nägele:** Writing – review & editing, Writing – original draft, Visualization, Validation, Supervision, Resources, Project administration, Investigation, Funding acquisition, Formal analysis, Conceptualization.

## Declaration of competing interest

The authors declare no conflict of interest.

## Acknowledgements

We thank the members of Plant Evolutionary Cell Biology at LMU München and the members of TRR175 for constructive discussions and advice. We thank Prof. Andreas Klingl for support with the TEM analysis. Further, we thank the Graduate School Life Science Munich (LSM) for support. This work was funded by Deutsche Forschungsgemeinschaft (DFG), TRR175/C01 and TRR175/D03.

## Supplementary materials

Supplementary material associated with this article can be found, in the online version, at doi:10.1016/j.stress.2025.100791.

## Data availability

Data of this study is available in the supplements and in a repository of the NFDI Data Plant consortium

## References

Braun, D.M., 2022. Phloem loading and unloading of sucrose: what a long, strange trip from source to sink. Annu Rev. Plant Biol. 73, 553–584.
Brauner, K., Hörmiller, I., Nägele, T., Heyer, A.G., 2014. Exaggerated root respiration accounts for growth retardation in a starchless mutant of Arabidopsis thaliana. Plant J. 79, 82–91.
Bruinsma, J., 1961. A comment on the spectrophotometric determination of chlorophyll. Biochim. Biophys. Acta 52, 576–578.
Dai, N., Schaffer, A., Petreikov, M., Shahak, Y., Giller, Y., Ratner, K., Levine, A., Granot, D., 1999. Overexpression of Arabidopsis hexokinase in tomato plants

inhibits growth, reduces photosynthesis, and induces rapid senescence. Plant Cell 11, 1253–1266.
Ding, X., Jimenez-Gongora, T., Krenz, B., Lozano-Duran, R., 2019. Chloroplast clustering around the nucleus is a general response to pathogen perception in *Nicotiana benthamiana*. Mol. Plant Pathol. 20, 1298–1306.
Ding, Y., Shi, Y., Yang, S., 2020. Molecular regulation of plant responses to environmental temperatures. Mol. Plant 13, 544–564.
Flügge, U.I., 1999. Phosphate translocators in plastids. Annu. Rev. Plant Physiol. Plant Mol. Biol. 50, 27–45.
Flügge, U.I., Heldt, H.W., 1981. The phosphate translocator of the chloroplast envelope. Isolation of the carrier protein and reconstitution of transport. Biochim. Biophys. Acta 638, 296–304.
Fürtauer, L., Pschenitschnigg, A., Scharkosi, H., Weckwerth, W., Nägele, T., 2018. Combined multivariate analysis and machine learning reveals a predictive module of metabolic stress response in Arabidopsis thaliana. Mol. Omics 14, 437–449.
Fürtauer, L., Weckwerth, W., Nägele, T., 2016. A benchtop fractionation procedure for subcellular analysis of the plant metabolome. Front. Plant Sci. 7, 1912.
Geigenberger, P., Thormählen, I., Daloso, D.M., Fernie, A.R., 2017. The unprecedented versatility of the plant thioredoxin system. Trends. Plant Sci. 22, 249–262.
Gibon, Y., Pyl, E.T., Sulpice, R., Lunn, J.E., Höhne, M., Günther, M., Stitt, M., 2009. Adjustment of growth, starch turnover, protein content and central metabolism to a decrease of the carbon supply when Arabidopsis is grown in very short photoperiods. Plant Cell Environ. 32, 859–874.
Gotoh, E., Suetsugu, N., Yamori, W., Ishishita, K., Kiyabu, R., Fukuda, M., Higa, T., Shirouchi, B., Wada, M., 2018. Chloroplast accumulation response enhances leaf photosynthesis and plant biomass production. Plant Physiol. 178, 1358–1369.
Govindjee, Shevela D, Björn, L.O., 2017. Evolution of the Z-scheme of photosynthesis: a perspective. Photosynth. Res. 133, 5–15.
Granot, D., Kelly, G., Stein, O., David-Schwartz, R., 2014. Substantial roles of hexokinase and fructokinase in the effects of sugars on plant physiology and development. J. Exp. Bot. 65, 809–819.
Guy, C., Kaplan, F., Kopka, J., Selbig, J., Hincha, D.K., 2008. Metabolomics of temperature stress. Physiol. Plant 132, 220–235.
Hannah, M.A., Wiese, D., Freund, S., Fiehn, O., Heyer, A.G., Hincha, D.K., 2006. Natural genetic variation of freezing tolerance in Arabidopsis. Plant Physiol. 142, 98–112.
Hincha, D.K., Zuther, E., Heyer, A.G., 2003. The preservation of liposomes by raffinose family oligosaccharides during drying is mediated by effects on fusion and lipid phase transitions. Biochim. Biophys. Acta 1612, 172–177.
Hoermiller, I.I., Funck, D., Schonewolf, L., May, H., Heyer, A.G., 2022. Cytosolic proline is required for basal freezing tolerance in Arabidopsis. Plant Cell Environ. 45, 147–155.
Holzinger, A., Buchner, O., Lutz, C., Hanson, M.R., 2007. Temperature-sensitive formation of chloroplast protrusions and stromules in mesophyll cells of Arabidopsis thaliana. Protoplasma 230, 23–30.
Hu, D-G, Sun, C.-H., Zhang, Q.-Y., An, J.-P., You, C.-X., Hao, Y.-J., 2016. Glucose sensor MdHXK1 phosphorylates and stabilizes MdbHLH3 to promote anthocyanin biosynthesis in apple. PLoS Genet. 12, e1006273.
Irieda, H., Takano, Y., 2021. Epidermal chloroplasts are defense-related motile organelles equipped with plant immune components. Nat. Commun. 12, 2739.
Jalili, V., Afgan, E., Gu, Q., Clements, D., Blankenberg, D., Goecks, J., Taylor, J., Nekrutenko, A., 2020. The Galaxy platform for accessible, reproducible and collaborative biomedical analyses: 2020 update. Nucleic. Acids Res. 48, W395–W402.
Jing, W., Uddin, S., Chakraborty, R., Van Anh, D.T., Macoy, D.M., Park, S.O., Ryu, G.R., Kim, Y.H., Cha, J.Y., Kim, W.-Y., Kim, M.G., 2020. Molecular characterization of HEXOKINASE1 in plant innate immunity. Appl. Biol. Chem. 63, 76.
Kagawa, T., Sakai, T., Suetsugu, N., Oikawa, K., Ishiguro, S., Kato, T., Tabata, S., Okada, K., Wada, M., 2001. Arabidopsis NPL1: a phototropin homolog controlling the chloroplast high-light avoidance response. Science 291, 2138–2141.
Kasahara, M., Kagawa, T., Oikawa, K., Suetsugu, N., Miyao, M., Wada, M., 2002. Chloroplast avoidance movement reduces photodamage in plants. Nature 420, 829–832.
Kitashova, A., Adler, S.O., Richter, A.S., Eberlein, S., Dziubek, D., Klipp, E., Nägele, T., 2023. Limitation of sucrose biosynthesis shapes carbon partitioning during plant cold acclimation. Plant Cell Environ. 46, 464–478.
Kitashova, A., Lehmann, M., Schwenkert, S., Münch, M., Leister, D., Nägele, T., 2024. Insights into physiological roles of flavonoids in plant cold acclimation. Plant J. https://doi.org/10.1111/tpj.17097.
Kitashova, A., Schneider, K., Fürtauer, L., Schröder, L., Scheibenbogen, T., Fürtauer, S., Nägele, T., 2021. Impaired chloroplast positioning affects photosynthetic capacity and regulation of the central carbohydrate metabolism during cold acclimation. Photosynth. Res. 147, 49–60.
Kleine, T., Nägele, T., Neuhaus, H.E., Schmitz-Linneweber, C., Fernie, A.R., Geigenberger, P., Grimm, B., Kaufmann, K., Klipp, E., Meurer, J., Mohlmann, T., Mühlhaus, T., Naranjo, B., Nickelsen, J., Richter, A., Ruwe, H., Schroda, M., Schwenkert, S., Trentmann, O., Willmund, F., Zoschke, R., Leister, D., 2021. Acclimation in plants - the Green Hub consortium. Plant J. 106, 23–40.
Knaupp, M., Mishra, K.B., Nedbal, L., Heyer, A.G., 2011. Evidence for a role of raffinose in stabilizing photosystem II during freeze-thaw cycles. Planta 234, 477–486.
Kodama, Y., Tsuboi, H., Kagawa, T., Wada, M., 2008. Low temperature-induced chloroplast relocation mediated by a blue light receptor, phototropin 2, in fern gametophytes. J. Plant Res. 121, 441–448.
Kong, S.G., Yamazaki, Y., Shimada, A., Kijima, S.T., Hirose, K., Katoh, K., Ahn, J., Song, H.G., Han, J.W., Higa, T., Takano, A., Nakamura, Y., Suetsugu, N., Kohda, D., Uyeda, T.Q.P., Wada, M., 2024. Chloroplast unusual positioning 1 is a plant-specific actin polymerization factor regulating chloroplast movement. Plant Cell 36, 1159–1181.
Kozakov, D., Hall, D.R., Xia, B., Porter, K.A., Padhorny, D., Yueh, C., Beglov, D., Vajda, S., 2017. The ClusPro web server for protein-protein docking. Nat. Protoc. 12, 255–278.
Love, M.I., Huber, W., Anders, S., 2014. Moderated estimation of fold change and dispersion for RNA-seq data with DESeq2. Genome Biol. 15, 550.
Maeda, H., Dudareva, N., 2012. The shikimate pathway and aromatic amino acid biosynthesis in plants. Annu Rev. Plant Biol. 63, 73–105.
Natesan, S.K., Sullivan, J.A., Gray, J.C., 2005. Stromules: a characteristic cell-specific feature of plastid morphology. J. Exp. Bot. 56, 787–797.
Nedo, A.O., Liang, H., Sriram, J., Razzak, M.A., Lee, J.Y., Kambhamettu, C., Dinesh-Kumar, S.P., Caplan, J.L., 2024. CHUP1 restricts chloroplast movement and effector-triggered immunity in epidermal cells. New. Phytol. 244, 1864–1881.
Nägele, T., 2022. Metabolic regulation of subcellular sucrose cleavage inferred from quantitative analysis of metabolic functions. Quant. Plant Biol. 3, e10.
Patzke, K., Prananingrum, P., Klemens, P.A.W., Trentmann, O., Rodrigues, C.M., Keller, I., Fernie, A.R., Geigenberger, P., Bolter, B., Lehmann, M., Schmitz-Esser, S., Pommerrenig, B., Haferkamp, I., Neuhaus, H.E., 2019. The plastidic sugar transporter pSuT influences flowering and affects cold responses. Plant Physiol. 179, 569–587.
Posit Team, 2024. RStudio: Integrated Development Environment for R. Posit Software. PBC, Boston, MA. URL. http://www.posit.co/.
Richter, A.S., Nägele, T., Grimm, B., Kaufmann, K., Schroda, M., Leister, D., Kleine, T., 2023. Retrograde signaling in plants: a critical review focusing on the GUN pathway and beyond. Plant Commun. 4, 100511.
Ruan, J., Zhou, Y., Zhou, M., Yan, J., Khurshid, M., Weng, W., Cheng, J., Zhang, K., 2019. Jasmonic acid signaling pathway in plants. Int. J. Mol. Sci. 20, 2479.
Sakai, T., Kagawa, T., Kasahara, M., Swartz, T.E., Christie, J.M., Briggs, W.R., Wada, M., Okada, K., 2001. Arabidopsis nph1 and npl1: blue light receptors that mediate both phototropism and chloroplast relocation. PNAS 98, 6969–6974.
Schwenkert, S., Fernie, A.R., Geigenberger, P., Leister, D., Möhlmann, T., Naranjo, B., Neuhaus, H.E., 2022. Chloroplasts are key players to cope with light and temperature stress. Trends. Plant Sci. 27, 577–587.
Serrano, M., Kanehara, K., Torres, M., Yamada, K., Tintor, N., Kombrink, E., Schulze-Lefert, P., Saijo, Y., 2012. Repression of sucrose/ultraviolet B light-induced flavonoid accumulation in microbe-associated molecular pattern-triggered immunity in Arabidopsis. Plant Physiol. 158, 408–422.
Seydel, C., Biener, J., Brodsky, V., Eberlein, S., Nagele, T., 2022. Predicting plant growth response under fluctuating temperature by carbon balance modelling. Commun. Biol. 5, 164.
Tanaka, H., Sato, M., Ogasawara, Y., Hamashima, N., Buchner, O., Holzinger, A., Toyooka, K., Kodama, Y., 2017. Chloroplast aggregation during the cold-positioning response in the liverwort Marchantia polymorpha. J. Plant Res. 130, 1061–1070.
Tang, Q., Xu, D., Lenzen, B., Brachmann, A., Yapa, M.M., Doroodian, P., Schmitz-Linneweber, C., Masuda, T., Hua, Z., Leister, D., Kleine, T., 2024. GENOMES UNCOUPLED PROTEIN1 binds to plastid RNAs and promotes their maturation. Plant Commun., 101069
Tian, F., Yang, D.C., Meng, Y.Q., Jin, J., Gao, G., 2020. PlantRegMap: charting functional regulatory maps in plants. Nucleic. Acids Res. 48, D1104–D1113.
Wada, M., Kong, S.G., 2018. Actin-mediated movement of chloroplasts. J. Cell Sci. 131.
Wang, Y., Mostafa, S., Zeng, W., Jin, B., 2021. Function and mechanism of Jasmonic Acid in plant responses to abiotic and biotic Stresses. Int. J. Mol. Sci. 22, 8568.
Wiese, A., Groner, F., Sonnewald, U., Deppner, H., Lerchl, J., Hebbeker, U., Flügge, U., Weber, A., 1999. Spinach hexokinase I is located in the outer envelope membrane of plastids. FEBS Lett. 461, 13–18.
Yanagisawa, S., Yoo, S.D., Sheen, J., 2003. Differential regulation of EIN3 stability by glucose and ethylene signalling in plants. Nature 425, 521–525.
Zhu, Z., An, F., Feng, Y., Li, P., Xue, L., A, M., Jiang, Z., Kim, J.M., To, T.K., Li, W., Zhang, X., Yu, Q., Dong, Z., Chen, W.Q., Seki, M., Zhou, J.M., Guo, H., 2011. Derepression of ethylene-stabilized transcription factors (EIN3/EIL1) mediates jasmonate and ethylene signaling synergy in Arabidopsis. Proc. Natl. Acad. Sci. U.S. A. 108, 12539–12544.